Tensile-Stress Dependence of Magnetic Hysteresis Properties Measured by the Acoustically Stimulated Electromagnetic Response in Steel

Yuhei Suzuki, Hisato Yamada, Kenji Ikushima

***Abstract*— Magnetic hysteresis properties are sensitive to stress in ferromagnetic materials. This suggests that magnetic measurements are a potential method to evaluate residual stress in steel products. Nevertheless, nondestructive inspection of residual stress by using magnetic properties has been limited because bulk properties over the entire sample are usually obtained in conventional hysteresis curve measurements through electromagnetic induction; thus, local hysteresis properties are not measured. However, the spatial mapping of local hysteresis properties has been demonstrated recently by ultrasound focusing and scanning. This technique is based on the generation and detection of the acoustically stimulated electromagnetic (ASEM) response. In this study, we investigate the stress dependence of local hysteresis loops through the ASEM response using a tensile testing machine and provide conversion coefficients to estimate tensile stress from the values of local hysteresis properties. The results indicate that hysteresis properties associated with coercivity, remanent magnetization, and hysteresis loss are promising parameters as an index for evaluating residual stress.**

***Index Terms*—Ultrasound, electromagnetic response, nondestructive evaluation, residual stress, steel.**

I. Introduction

STEEL is a major component used in machines, automobiles, buildings, and infrastructure. Undesirable residual stress is usually introduced during the manufacturing of steel materials, product fabrication, and welding. When service stress is combined with initial residual stress, the concentration of tensile stresses may damage engineering components [1]-[3]. To avoid the risk of damage, it is important to understand the stress distribution in actual objects. This information allows early repairs, and guides design and fabrication. Generally, the residual stress is obtained by measuring strain relaxation using the destructive sectioning method [4] or semi-destructive hole-drilling method [5], [6]. X-ray diffraction is used for a nondestructive stress evaluation, but the method is limited to steel materials with small crystal grains [7]-[9]. Although stress inspection techniques using conventional ultrasound or magnetic measurements have also been studied [10]-[14], nondestructive quantitative evaluation of residual stress and its spatial mapping are still being developed.

Ferromagnetic materials exhibit hysteresis in the variation of flux density B with magnetic field H. Hysteretic properties, such as permeability, coercivity, remanent magnetization, and hysteresis loss, are sensitive to stress produced in the ferromagnetic materials [15]-[17]. Consequently, magnetic measurements could be used to evaluate residual stress in steel materials. However, the use of magnetic properties for stress evaluation has been limited because bulk properties over the entire sample are obtained in conventional hysteresis curve ($B-H$ curve) measurements through electromagnetic induction; thus, the local hysteresis properties are not probed.

However, the spatial mapping of local magnetic hysteresis behaviors has become possible by ultrasonic focusing and scanning [18]-[20]. This technique is based on the generation and detection of the acoustically stimulated electromagnetic (ASEM) response. In the ASEM method, the specimen is locally interrogated with ultrasound which modulates the magnetic polarization [18]-[22]. The electromagnetic response emitted from the ultrasonic focal spot is detected using a narrow-band tuned antenna. The first harmonic component of the radio frequency (rf) equals the ultrasonic excitation frequency. One of the advantages of this method is that the spatial resolution is determined by ultrasonic focusing, not by magnetic field focusing. Thus, well-defined spatial mapping of magnetic properties is achieved. The signal intensity of the ASEM response is expressed by a piezomagnetic coefficient, d_{loc}, in the acoustically excited local area of the object [18]-[20]. The hysteresis curve of the ASEM intensity corresponds to that of $d_{\mathrm{loc}}(H)$. Thus, we assume that the ASEM hysteresis curve is sensitive to tensile stress. In this study, we clarify the tensile stress dependence of the ASEM hysteresis curve in steel and provide guidelines for quantitative stress evaluation by using the ASEM method.

II. Method

A. Theoretical background

Because the acoustic pressure is on the order of 10 kPa, the stress-induced magnetization shows a linear response [18]. Biased magnetostriction is phenomenologically equivalent to

This work was financially supported by JSPS KAKENHI Grant Number JP17H02808.

Y. Suzuki is with the Department of Applied Physics, Tokyo University of Agriculture and Technology, Tokyo 184-8588, Japan (e-mail: s175294y@st.go.tuat.ac.jp) and also with the instrumentation division of IHI Inspection & Instrumentation Co., Ltd., Kanagawa 236-0004, Japan.

H. Yamada is with the Department of Applied Physics, Tokyo University of Agriculture and Technology, Tokyo 184-8588, Japan (e-mail: h-yamada@cc.tuat.ac.jp).

K. Ikushima is with the Department of Applied Physics, Tokyo University of Agriculture and Technology, Tokyo 184-8588, Japan (e-mail: ikushima@cc.tuat.ac.jp).

piezomagnetism in the linear response regime [23], and we do not distinguish them in this discussion. The linear response equation for magnetomechanical coupling is expressed as (i, j = 1, 2, …, 6 and k, m = 1, 2, 3)

$$S_i = \left(\partial S_i/\partial T_j\right)_H T_j + (\partial S_i/\partial H_m)_T H_m,$$
$$B_m = (\partial B_m/\partial T_i)_H T_i + (\partial B_m/\partial H_k)_T H_k, \quad (1)$$

where S, T, H, and B are the strain, stress, magnetic field, and magnetic flux density components, respectively. The coefficients relating the quantities $d_{mi} = (\partial B_m/\partial T_i)_H$ and $\mu_{mk} = (\partial B_m/\partial H_k)_T$ are the piezomagnetic constant and permeability constant, respectively. The magnetic flux density, B, is expressed by a nonlinear hysteresis function, $B(H,T)$. When the acoustic stress, $T(t)$, is applied to a ferromagnetic material, the magnetic flux density, $B(t)$, is temporally modulated through Eq. (1). Consequently, an alternating dipolar field is emitted to the surrounding environment [18]. Therefore, the ASEM signal voltage, V_{sig}, detected with a tuned loop antenna, is

$$V_{\mathrm{sig}} = \eta(dB_m/dt) = \eta d_{mi}(dT_i/dt), \quad (2)$$

where η is the detection efficiency in the measurements.

In general, the piezomagnetic coefficient can be extended to a complex number [20]. When the acoustic stress, $T(\omega_0) = T_0 e^{-i\omega_0 t}$, is applied to a local area in material, the induced flux density is written as $B(\omega_0, H) = B_0 e^{-i(\omega_0 t - \delta(H))}$, where $\delta(H)$ is the phase delay of B with respect to T. From the ratio of $B(\omega_0, H)$ and $T(\omega_0)$, the local piezomagnetic coefficient, $d_{\mathrm{loc}}(H)$, at ω_0 is expressed as

$$d_{\mathrm{loc}}(H) = \frac{B_0(H)}{T_0}[\cos\delta(H) + i\sin\delta(H)] = d'(H) + id''(H). \quad (3)$$

The phase delay, δ, gives rise to the imaginary part, d'', characterizing the energy loss at ω_0.

Next, we describe the relation between ASEM signals and the complex piezomagnetic coefficients. From Eq. (2), the ASEM signal, V_{sig}, is written as

$$V_{\mathrm{sig}}(t, H) = \eta\frac{dB(t, H)}{dt} = \eta\frac{1}{2\pi}\int_{-\infty}^{\infty}(-i\omega)B(\omega, H)e^{-i\omega t}d\omega\,. \quad (4)$$

The Fourier component, $V_{\mathrm{sig}}(\omega, H)$, is written as

$$V_{\mathrm{sig}}(\omega, H) = -i\eta\omega B(\omega, H) = -i\eta\omega d(\omega, H)T(\omega) = \eta\omega[d''(\omega, H) - id'(\omega, H)]T(\omega), \quad (5)$$

where $V_{\mathrm{sig}}(\omega, H)$ has a quadrature phase shift with respect to $B(\omega, H)$ induced in a material. Consequently, for a sinusoidal wave, $T(\omega_0) = T_0 e^{-i\omega_0 t}$, the first-harmonic component of $V_{\mathrm{sig}}(\omega, H)$ is expressed as

$$V_{\mathrm{sig}}(\omega, H) = \eta\omega B_0(H)e^{-i(\omega_0 t - \delta(H) - \phi + \pi/2)}, \quad (6)$$

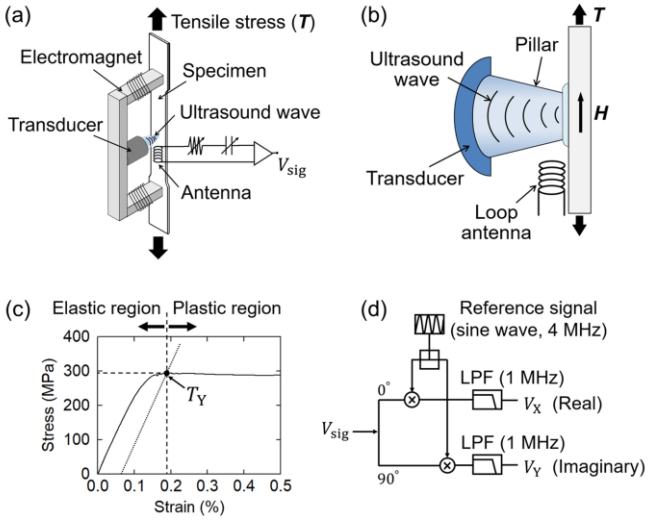

Fig. 1. (a) Schematic of the in situ measurement setup in tensile testing. (b) Schematic of the configuration of the transducer and loop antenna. (c) Tensile stress-strain curve of a steel plate (S25C). (d) Block diagram of the numerical PSD scheme.

where ϕ is the adjustable phase shift attributed to the measurement system. Using a phase-sensitive detection (PSD) scheme, we separate $V_{\mathrm{sig}}(\omega, H)$ into the in-phase component, V_{X} (real part), and the quadrature component, V_{Y} (imaginary part). When ϕ is tuned to $\pi/2$, these components are written as

$$V_{\mathrm{X}} = \eta\omega_0 B_0(H)\cos\delta(H) = \eta\omega_0 T_0 d'(H)\,, \quad (7)$$

$$V_{\mathrm{Y}} = \eta\omega_0 B_0(H)\sin\delta\,(H) = \eta\omega_0 T_0 d''(H). \quad (8)$$

The in-phase component ($V_{\mathrm{X}} \propto d'$) is a quasi-static loss with respect to magnetomechanical effects. The quadarature component ($V_{\mathrm{Y}} \propto d''$) is attributed to energy dissipation processes, such as microscopic eddy current effects induced by domain wall movement [19], [24]-[26].

B. Sample preparation

Tensile testing samples (size: 490 × 70 × 6 mm) were machined from 25-mm-thick carbon steel plates (S25C, JIS G4051:2009). Recrystallization and grain deformation occur during the rolling process of steelmaking and the magnetic easy axis in individual grains tends to be aligned along rolling direction $\boldsymbol{R}$ [27]-[29]. The alignment of grains may cause the mechanical and magnetic anisotropies. Thus, we prepared two samples (Sample $\mathrm{I}_{//}$ and $\mathrm{II}_{\perp}$). Rolling directions $\boldsymbol{R}$ of Samples $\mathrm{I}_{//}$ and $\mathrm{II}_{\perp}$ were parallel and perpendicular to the longitudinal direction of the steel plate, respectively. A reference sample was also prepared for the destructive measurement of the stress-strain curve, in which the rolling direction was parallel to the longitudinal direction of the plate.

C. Measurement setup

Schematics of the in situ measurement setup for tensile testing are shown in Figs. 1(a) and 1(b). ASEM measurements were performed using a 4 MHz focusing transducer (Japan Probe Co., Ltd.) with a delay line (27-mm-long polystyrene pillar) for separating the transducer excitation pulse from the

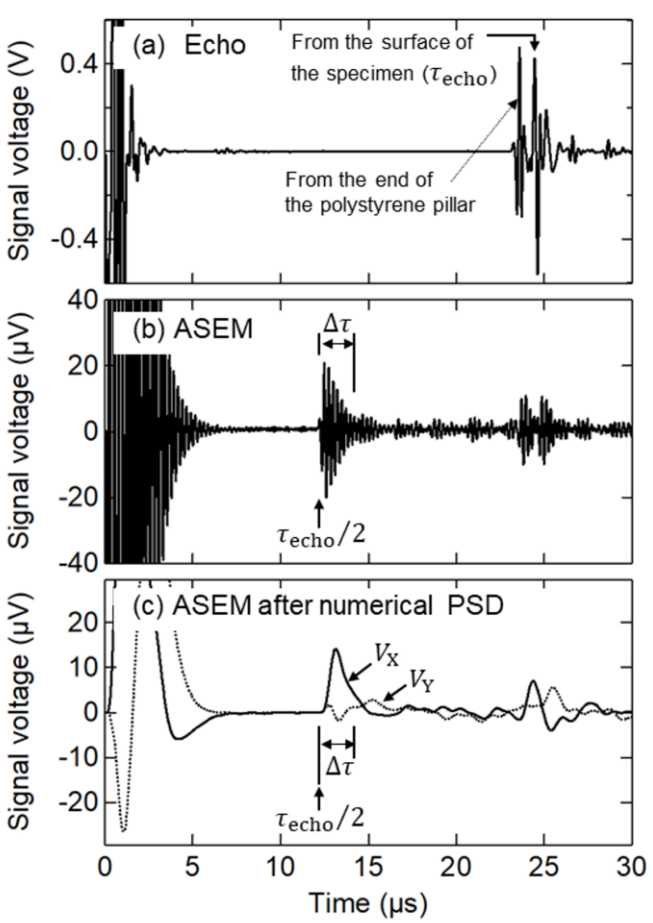

Fig. 2. (a) Real-time echo waveform. (b) Real-time ASEM waveform. (c) The in-phase component, V_X (solid line), and the quadrature component, V_Y (dotted line), after numerical PSD.

ASEM signals [21]. The diameter of the focal spot size was about 1.7 mm. The signal was detected by a resonant loop antenna tuned at 4.1 MHz. The tensile testing samples were subjected to external magnetic fields along the longitudinal direction of the plates by using a commercial electromagnet. The external magnetic fields were calculated from $H = NI/L$ where N, I, and L are the total number of turns (400 turns), the applied electric current, and the length of a magnetic circuit composed of the electromagnet and the sample (470 mm), respectively.

The stress-strain curve measured in the reference sample is shown in Fig. 1(c). The yield stress point, T_Y, for the reference sample was estimated to be 290 MPa.

Typical real-time waveforms obtained by in situ measurements are shown in Fig. 2. The echo signal from the surface of steel was observed at τ_{echo} = 24.4 μs (Fig. 2(a)). The direct rf signal, $V_{sig}(t)$, of the ASEM response was observed at half of the echo delay time ($\tau_{echo}/2$ = 12.2 μs) (Fig. 2(b)). Using a PSD scheme (Fig. 1(d)), the direct rf signal was numerically converted to the PSD signal. The ASEM waveforms after PSD are shown in Fig. 2(c).

In the hysteresis measurements, the signal voltages for $V_{sig}(t)$, $V_X(t)$, and $V_Y(t)$ were plotted as the time-averaged intensities, the amplitude, $|\overline{V_{sig}}| = \sqrt{(V_X)^2 + (V_Y)^2}$, the in-phase component, $\overline{V_X}$, and the quadrature component, $\overline{V_Y}$, integrated between $\tau_{echo}/2$ and $\tau_{echo}/2 + \Delta\tau$ [19], [20]. The integration time, $\Delta\tau$, was set to 2 μs. In the initial state of the hysteresis measurements, the specimen was demagnetized by applying an alternating current with the electromagnet.

III. Results and Analysis

Figures 3(a)–3(f) show the hysteresis curves of the amplitude, $|\overline{V_{sig}}|$, obtained for the in situ measurements of Sample $I_{//}$. Plastic deformation behavior was observed when the stress was fixed at 333 MPa, where the strain continued to increase even though the applied stress was fixed. Thus, the yield stress point for Sample $I_{//}$, $T_Y^{I_{//}}$, was between 292 and 333 MPa, which agrees with the value of the reference sample. Similarly, the yield stress point for Sample $II_{\perp}$, $T_Y^{II_{\perp}}$, was between 250 and 292 MPa for the in situ measurements and was similar to that of Sample $I_{//}$. Because the original steel plate from the steel manufacturer was relatively thick (thickness: 25 mm), The alignment of grains arising from rolling was probably small in the prepared samples. The hysteresis curve clearly depended on the applied tensile stress (Figs. 3(a)–3(f)). The stress dependence would be clearer in the loop structure of the in-phase component, $\bar{V}_X(H)$. Figures 3(g)–3(l) show the hysteresis curves of $\bar{V}_X(H)$ and $\bar{V}_Y(H)$ for individual fixed stresses. Because the quadrature component, $\bar{V}_Y$, is negligible in the samples, we focus on hysteresis parameters obtained from the $\bar{V}_X$ loop.

The hysteresis parameters are defined in Fig. 3(g). The coercivity, H_c, and the remanent magnetization signal, V_r, are determined from the intercepts of the transversal and longitudinal axes in the $\bar{V}_X(H)$ hysteresis loop, respectively. The signal voltage, V_r, is the ASEM intensity arising from the remanent magnetization. We introduce two further parameters, the area of the hysteresis loop, W, and the initial slope of the initial magnetization curve, m_0. The area is written as $W = \oint \bar{V}_X(H)dH \propto \oint d'(H)dH = \oint \left(\frac{dB}{dT}\right) dH \approx \frac{d}{dT}\oint BdH = \frac{d}{dT}W_{B-H}$, where W_{B-H} corresponds to the hysteresis loss in the standard $B-H$ curve. Similarly, the initial slope is written as $m_0 = \frac{d\bar{V}_X}{dH} \propto \frac{d}{dH}d'(H) = \frac{d^2}{dHdT}B \approx \frac{d}{dT}\mu'(T)$, where μ' is the real part of the complex permeability.

The stress dependence of the coercivity, $H_c(T)$, is shown in Fig. 4. No significant difference between Samples $I_{//}$ and $II_{\perp}$ was observed in the stress dependence. The coercivity, $H_c(T)$, decreased quadratically in the elastic region as tensile stress increased. Thus, a well-defined conversion function from coercivity to tensile stress was derived. Beyond the yield stress point, the hysteresis curve was insensitive to the stress. We explain this result as follows. In the plastic region, the deformation continues to increase as the internal stress is released, and thus the internal stress no longer increases as externally applied stress is increased.

Because the signal voltage of the ASEM response depends

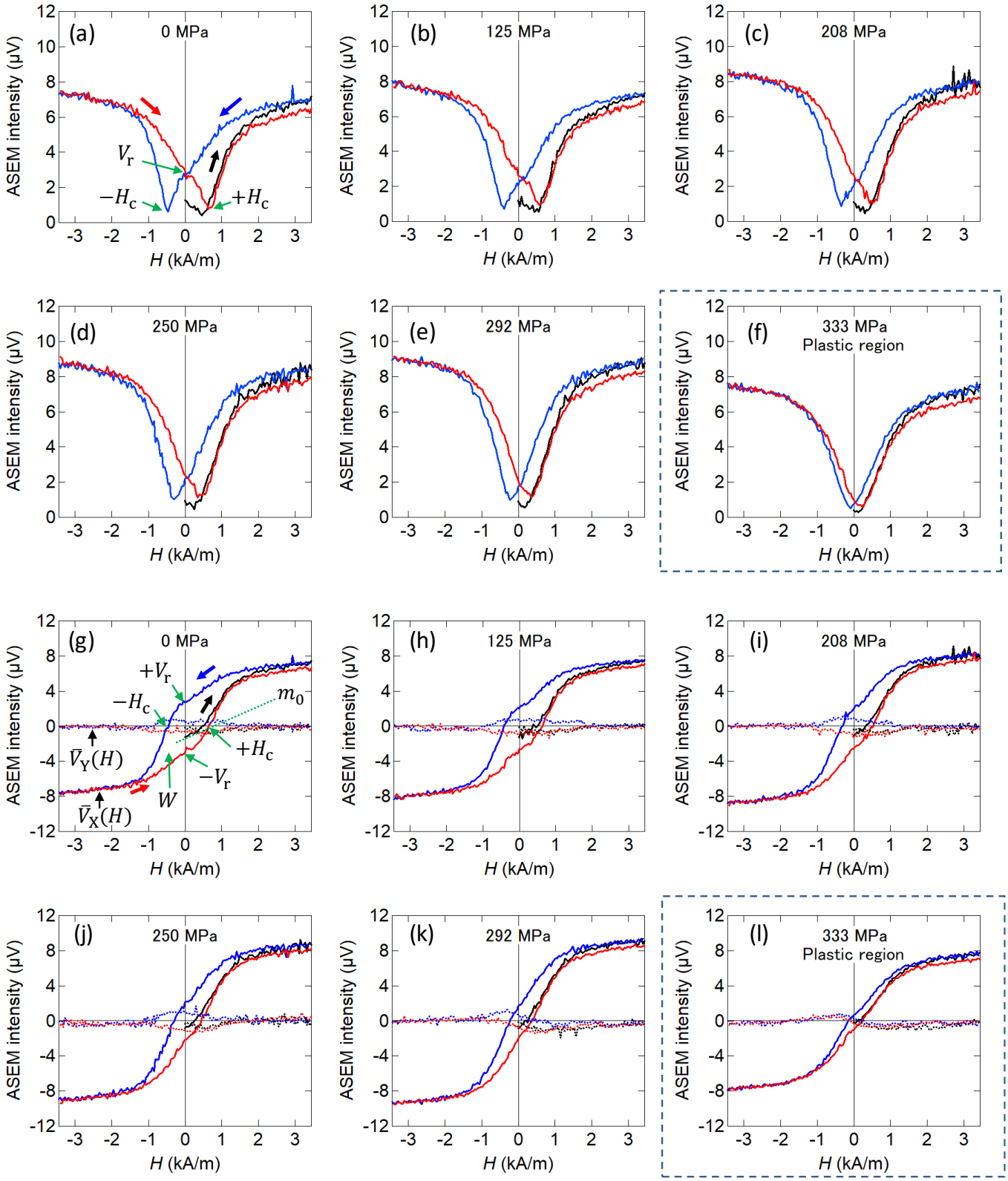

Fig. 3. Hysteresis curves of Sample $I_{//}$. (a)–(f) $\bar{V}_{sig}(H)$. (g)–(l) The in-phase component, $\bar{V}_X(H)$ (solid line), and the quadrature component, $\bar{V}_Y(H)$ (dotted line). The black, blue, and red lines represent the initial magnetization curve, the downward-field curve, and the upward-field curve, respectively. The data in (f) and (l) show the hysteresis curves in the plastic region beyond the yield stress point.

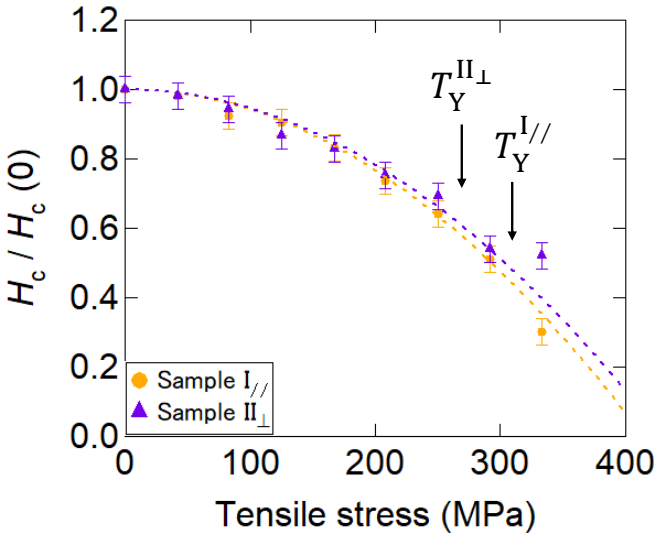

Fig. 4. Stress dependence of the normalized coercivity, $H_c/H_c(T=0)$. The dotted line shows the best-fit curve below the yield stress points.

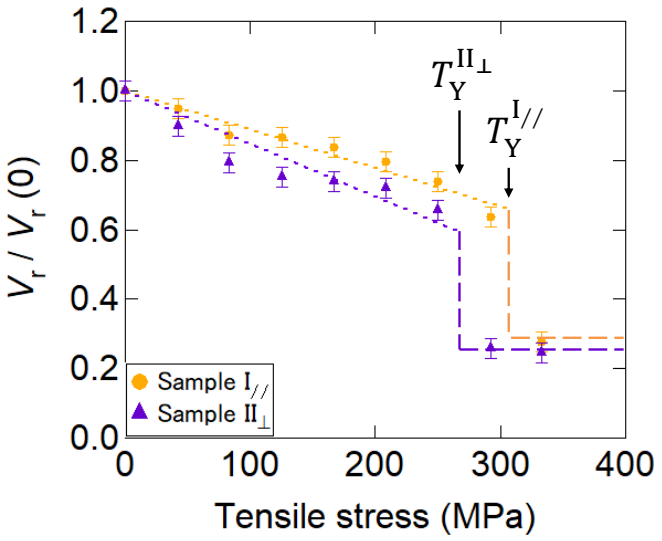

Fig. 5. Stress dependence of the normalized remanent signal, $V_r/V_r(T=0)$. The dotted line shows the best-fit curve below the yield stress points. The dashed line is a guide to the eye.

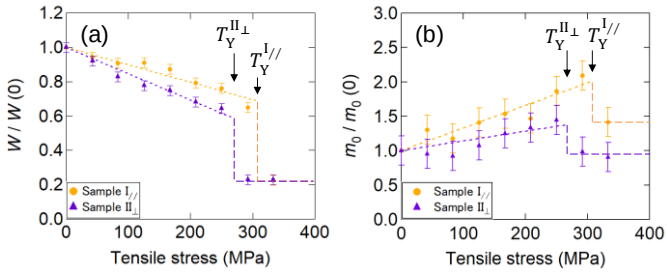

Fig. 6. Stress dependence of (a) the normalized area of loops, $W/W(T=0)$, and (b) the normalized slope, $m_0/m_0(T=0)$, of the initial magnetization curve. The dotted line shows the best-fit curve below the yield stress points. The dashed line is a guide to the eye.

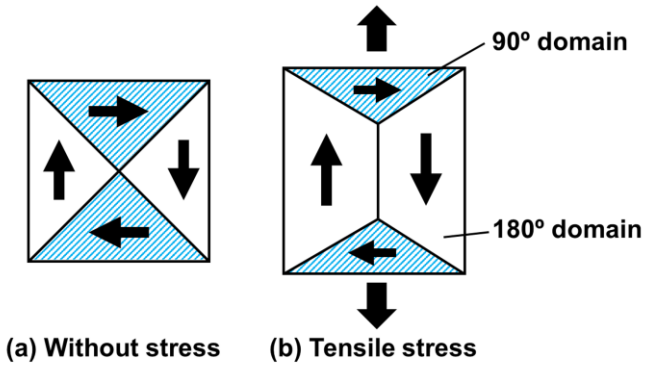

Fig. 7. Schematics of movement of the 180° domains and the 90° domains (a) without stress and (b) under tensile stress.

on acoustic pressure or the incident angle of ultrasound irradiation, the ASEM intensity is sensitive to the measurement setting. We should note that the coercivity does not depends on the signal voltage of ASEM response and the conditions of ultrasound irradiation. However, it is necessary to keep the conditions of ultrasound irradiation constant in the whole mapping area when we attempt to obtain the stress mapping from the values of V_r. The conditions can be confirmed by measuring the echo delay time and echo signal intensity. A mechanical feedback system that adjusts the distance and angle of the probe via echo signals will be needed for the stress mapping through V_r. Here, we discuss the stress dependence of $V_r(T)$, $W(T)$, and $m_0(T)$ by using the normalized ASEM intensity divided by the value at zero stress (Figs. 5 and 6).

As with the coercivity, the remanent magnetization signal, $V_r(T)$, is a decreasing function of tensile stress. Accordingly, the hysteresis loop area, $W(T)$, also monotonically decreases with increasing tensile stress. The initial slope, $m_0(T)$, tends to increases with increasing stress.

IV. Discussion

We obtained the stress dependence of local magnetic hysteresis in steel from the ASEM response. Particularly, the coercivity is the most promising hysteresis parameter as an index of the quantitative evaluation of stress. The coercivity is usually affected by micro defects and domain wall motion. In the elastic deformation region, no new defects are introduced by applying stress. Thus, domain wall motion plays a dominant role in the stress dependence of coercivity.

Here, we discuss domain wall motion under tensile stress qualitatively based on the Gibbs free energy, as proposed by Landau and Lifshitz [30]. The domain structure of a material results from the minimization of the Gibbs free energy, consisting of exchange energy, magnetostatic energy, magnetoelastic anisotropy energy, magnetocrystalline anisotropy energy, and Zeeman energy. When stress is a variable, the magnetoelastic anisotropy energy, E_T, is an important term in the total free energy. The magnetoelastic anisotropy energy is expressed as $E_T = -3/2\,\lambda T\cos^2\theta$ for isotropic magnetostriction, where T (>0) is tensile stress, λ is the magnetostrictive coefficient, and θ is the angle between the

magnetization and stress direction [31], [32]. Because of the positive magnetostriction ($\lambda > 0$) in steel, applying tensile stress reduces E_T. In addition, when the tensile stress is applied in the direction of the external magnetic field, the magnetization tends to be oriented to the direction of the tensile stress (i.e., $\theta \to 0$) owing to the minimization of E_T [32], [33]. Therefore, under tensile stress, the volume of the 180° domains increases, whereas that of the 90° domains decreases (Fig. 7) [32]-[34]. Because the movement of the 180° domains occurs at lower magnetic fields compared with that of the 90° domains [35], [36], the extension of the 180° domains decreases H_c, V_r, and W and increases the initial slope m_0.

The conversion coefficients between these hysteresis parameters and tensile stress, T, are necessary for quantitative stress evaluation. We fitted the stress characteristic curves of the normalized hysteresis parameters, $H_\mathrm{c}/H_\mathrm{c}(T=0)$, $V_\mathrm{r}/V_\mathrm{r}(T=0)$, $W/W(T=0)$, and $m_0/m_0(T=0)$ (Figs. 4–6), to a function of the power of stress, $1 + C_1T + C_2T^2$, with a single fitting parameter as $C_1 = 0$ for H_c and $C_2 = 0$ for the other parameters. The stress evaluation in the elastic region near the yield stress point is the most important for practical applications. In the measured sample, it was between 150 and 250 MPa. The best-fit parameters in the elastic region were evaluated to be $C_2 = -5.83 \times 10^{-18}$ Pa^{-2}(-5.42×10^{-18} Pa^{-2}) for H_c, $C_1 = -1.11 \times 10^{-9}$ Pa^{-1} (-1.52×10^{-9} Pa^{-1}) for V_r, $C_1 = -1.02 \times 10^{-9}$ Pa^{-1}(-1.54×10^{-9} Pa^{-1}) for W, and $C_1 = 3.29 \times 10^{-9}$ Pa^{-1}(1.42×10^{-9} Pa^{-1}) for m_0 for Sample $\mathrm{I}_{//}$ (Sample $\mathrm{II}_{\perp}$). The coercivity, H_c, is the most suitable parameter for quantitative evaluation in the elastic region. In contrast, the drastic drop of V_r and W at the yield stress point may be suitable for identifying plastically deformed areas in steel.

V. Conclusion

We have measured the stress dependence of magnetic hysteresis properties in carbon steel using the ASEM method. The hysteresis parameters, such as the coercivity and remanent magnetization signal, decreased monotonically as a function of tensile stress in the elastic region. When the tensile stress exceeded the yield stress point, the hysteresis parameters decreased drastically. We obtained the conversion coefficients for converting the hysteresis parameters to tensile stress. Probing the local hysteresis properties via ultrasound excitation provides a new method for the nondestructive evaluation of residual stress.

Acknowledgment

We thank T. Uchida from Nippon Pneumatic Mfg. Co., Ltd. (NPK) for preparing the samples. We also thank T. Ozaki from Denshijiki Industry Co., Ltd. and Y. Ichikawa from Tokyo University of Agriculture and Technology for technical help and experimental assistance.

References

[1] P. J. Withers and H. K. D. H. Bhadeshia, "Residual stress. Part 1 - Measurement techniques," *Mater. Sci. Technol.*, vol. 17, no. 4, pp. 355–365, Apr. 2001.

[2] P. J. Withers and H. K. D. H. Bhadeshia, "Residual stress. Part 2 - Nature and origins," *Mater. Sci. Technol.*, vol. 17, no. 4, pp. 366–375, Apr. 2001.

[3] G.S. Schajer and C. O. Ruud, "Overview of residual stresses and their measurement," in *Practical Residual Stress Measurement Methods*, Chichester, UK, John Wiley & Sons, 2013, pp. 1-27.

[4] N. Tebedge, G. Alpsten, and L. Tall, "Residual-stress measurement by the sectioning method," *Exp. Mech.*, vol. 13, no. 2, pp. 88–96, Feb. 1973.

[5] B. Zuccarello, "Optimal calculation steps for the evaluation of residual stress by the incremental hole-drilling method", *Exp. Mech.*, vol. 39, no. 2, pp. 117–124, Jun. 1999.

[6] D. George and D. J. Smith, "Through thickness measurement of residual stresses in a stainless steel cylinder containging shallow and deep weld repairs," *Int. J. Pres. Ves. Pip.*, vol. 82, no. 4, pp. 279–287, Apr. 2005.

[7] *Residual Stress Measurement by X-ray Diffraction. SAE J784, Society of Automotive Engineers Handbook Supplement*, SAE International, Warrendale, PA, USA, 2003.

[8] K. Hiratsuka, T. Sasaki, K. Seki, and Y. Hirose, "Development of measuring system for stress by means of image plate for laboratory x-ray experiment, " *JCPDS-International Centre for Diffraction Data*, vol. 46, pp. 61-67, 2003.

[9] I. C. Noyan and J. B. Cohen, *Residual stress: measurement by diffraction and Interpretation*, New York, NY, USA, Springer, 1987, p. 94.

[10] T. Leon-Salamanca and D. F. Bray, "Residual stress measurement in steel plates and welds using critically refracted longitudinal ($\mathrm{L_{CR}}$) waves," *Res. Nondestruct. Eval.*, vol. 7, no. 4, pp. 169–184, Dec. 1996.

[11] S. Abuku, "Magnetic Studies of Residual stress in iron and steel induced by uniaxial deformation," *Jpn. J. Appl. Phys.*, vol. 16, no. 7, pp. 1161-1170, 1977.

[12] A. Mitra, L. B. Sipahi, M. R. Govindaraju, D. C. Jiles, and V. R. V. Ramanan, "Effects of tensile stress on magnetic Barkhausen emissions in amorphous Fe-Si-B alloy," *J. Magn. Magn. Mater.*, vol. 153, no. 1-2, pp. 231–234, Feb. 1996.

[13] T. Inaguma, H. Sakamoto, and M. Hasegawa, "Stress dependence of Barkhausen noise in spheroidized cementite carbon steel," *IEEE Trans. Magn.*, vol. 49, no. 4, pp. 1310–1317, Apr. 2013.

[14] J. W. Wilson, G. Y. Tian, and S. Barrans, "Residual magnetic field sensing for stress measurement," *Sens. Actuators A: Phys.*, vol. 135, no. 2, pp. 381-387, Apr. 2007.

[15] D. Jiles, *Introduction to Magnetism and Magnetic Materials*, 3rd ed., Boca Raton, FL, USA, CRC Press, 2016, p. 421.

[16] S. Abuku and B. D. Cullity, "A magnetic method for the determination of residual stress," *Exp. Mech.*, vol. 11, no. 5, pp. 217-223, May 1971.

[17] J. M. Makar and B. K. Tanner, "The effect of plastic deformation and residual stress on the permeability and magnetostriction of steels," *J. Magn. Magn. Mater.*, vol. 222, no. 3, pp. 291-304, Dec. 2000.

[18] H. Yamada, K. Takashima, K. Ikushima, H. Toida, M. Sato, and Y. Ishizawa, "Magnetic sensing via ultrasonic excitation," *Rev. Sci. Instrum.*, vol. 84, no. 4, pp. 044903(1-5), 2013.

[19] H. Yamada, K. Watanabe, and K. Ikushima, "Magnetic hysteresis and magnetic flux patterns measured by acoustically stimulated electromagnetic response in a steel plate," *Jpn. J. Appl. Phys.*, vol. 54, no. 8, pp. 086601(1-4), 2015.

[20] H. Yamada, J. Yotsuji, and K. Ikushima, "Phase-sensitive detection of acoustically stimulated electromagnetic response in steel," *Jpn. J. Appl. Phys.*, vol. 57, no. 7S1, pp. 07LB09(1-5), 2018.

[21] K. Ikushima, S. Watanuki, and S. Komiyama, "Detection of acoustically induced electromagnetic radiation", *Appl. Phys. Lett.*, vol. 89, no. 19, pp. 194103(1-3), 2006.

[22] Y. Suzuki, H. Yamada, T. Ozaki, and K. Ikushima, "Stress dependence of magnetic hysteresis properties through acoustically stimulated electromagnetic response in steel," in *Proc. IEEE Int. Ultrason. Symp. (IUS)*, Oct. 2018, pp. 1–4.

[23] D. A. Berlincourt, D. R. Curran, and H. Jaffe, "Piezoelectric and Piezomagnetic Materials and Their Function in Transducers," in *Physical*

Acoustics, New York, USA, Academic Press, 1964, vol. 1, Part A, pp. 169-270.

[24] G. Bertotti, "Space‐time correlation properties of the magnetization process and eddy current losses: Applications. I. Fine wall spacing," *J. Appl. Phys.*, vol. 55, no. 12, pp. 4339-4347, 1984.

[25] G. Bertotti, " Physical interpretation of eddy current losses in ferromagnetic materials. I. Theoretical considerations," *J. Appl. Phys.*, vol. 57, no. 6, pp. 2110-2117, 1985.

[26] D. Jiles, "Frequency dependence of hysteresis curves in conducting magnetic materials," *J. Appl. Phys.*, vol. 76, no. 10, pp. 5849-5855, 1994.

[27] Y. Shimizu, Y. Ito, and Y. Iida, "Formation of the Goss orientation near the surface of 3 pct silicon steel during hot rolling," *Metall. Trans. A*, vol. 17, no. 8, pp. 1323-1334, Aug. 1986.

[28] D. Dorner, S. Zaefferer, L. Lahn, and D. Raabe, "Overview of microstructure and microtexture development in grain-oriented silicon steel," *J. Magn. Magn. Mater.*, vol. 304, no. 2, pp. 183-186, Sep. 2006.

[29] H. Kikuchi, I. Shimizu, K. Sato, and K. Iwata, "Nondestructive evaluation of material degradation and sub-millimeter sized defect detection in steel using magnetic measurements," *Case Stud. Nondestruct. Test. Eval.*, vol. 1, pp. 25-31, Apr. 2014.

[30] I. D. Landau and E. M. Lifshitz, *Physik Z.*, Sowjetunion, vol. 8, 153, 1935.

[31] R. Langman, "Magnetic properties of mild steel under conditions of biaxial stress," *IEEE Trans. Magn.*, vol. 26, no. 4, pp. 1246-1251, Jul. 1990.

[32] T. Liu, H. Kikuchi, K. Ara, Y. Kamada, and S. Takahashi, "Magnetomechanical effect of low carbon steel studied by two kinds of magnetic minor hysteresis loops," *NDT&E Int.*, vol. 39, no. 5, pp. 408-413, Jul. 2006.

[33] C. G. Stefanita, D. L. Atherton, and L. Clapham, "Plastic versus elastic deformation effects on magnetic Barkhausen noise in steel," *Acta Mater.*, vol. 48, no. 13, pp. 3545–3551, Aug. 2000.

[34] X. Kleber and A. Vincent, "On the role of residual internal stresses and dislocations on Barkhausen noise in plastically deformed steel," *NDT&E Int.*, vol. 37, no. 6, pp. 439-445, Sep. 2004.

[35] S. Chikazumi, *Physics of Ferromagnetism*, 2nd ed., New York, NY, USA, Oxford Univ. Press, 2009, p. 468.

[36] M. S. Amiri, M. Thielen, M. Rabung, M. Marx, K. Szielasko, and C. Boller, "On the role of crystal and stress anisotropy in magnetic Barkhausen noise," *J. Magn. Magn. Mater*., vol. 372, pp. 16-22, Dec. 2014.

Yuhei Suzuki was born in Shizuoka, Japan, in January 1985. He received the B.S. and M.S. degrees in Electrical engineering from Hosei University, Tokyo, Japan in 2011. He is currently working for IHI Inspection & Instrumentation Co., Ltd. in the instrumentation division for steel inspection. He is also pursuing the Ph.D. degree in electronic and information engineering at Tokyo University of A & T, Tokyo, Japan. His research interests include inspection of residual stress using hole-drilling methods and ultrasound techniques.

Hisato YAMADA received the B.S. and the M.S. degrees in applied physics from Tokyo University of A & T, Tokyo, Japan in 2011. He received the Ph.D. in electronic and information engineering from Tokyo University of A & T in 2014.

He is currently a postdoctoral fellow with Tokyo University of A & T. His research interests include magnetism, magnetomechanical coupling of materials, noninvasive sensing technology using ultrasound waves.

Kenji IKUSHIMA received the B.S. degree in applied physics from Waseda University, Tokyo, Japan in 1993 and the M.S. degree in physics from The University of Tokyo, Japan in 1996. He received the Ph.D. in physics from The University of Tokyo, Japan in 1999. From 1999 to 2000, he was a postdoctoral fellow with Japan Atomic Energy Research Institute (JAERI). From 2000 to 2008, he was a Research Assistant with Department of Basic Science, The University of Tokyo. Since 2008, he has been an Associate Professor with the Department of Applied Physics, Tokyo University of A & T. He is the author of more than 60 articles and more than 30 inventions. His research interests include magnetism and magnetic resonance, semiconductor quantum devices, nanomaterials, and noninvasive sensing technology using terahertz or ultrasound waves.